2016 American Control Conference (ACC)
Boston Marriott Copley Place
July 6-8, 2016. Boston, MA, USA

Tightly Coupled Integrated Inertial and Real-Time-Kinematic Positioning Approach Using Nonlinear Observer

Jakob M. Hansen[1], Tor Arne Johansen[1] and Thor I. Fossen[1]

Abstract— **Tightly coupled integration of inertial measurements and raw global navigation satellite measurements using a nonlinear observer is proposed for real-time-kinematic applications. The position, linear velocity and attitude estimates of a rover is aided by global pseudo-range and carrier-phase measurements from the rover and a base station. The tight integration is achieved using a modular observer design, where the attitude observer with gyro bias estimate is based on a nonlinear complementary filter. Two translational motion observers estimating position and linear velocity using single- or double-differenced range measurements, respectively, are presented. The range measurements include pseudo-range and carrier-phase measurements from the satellite constellation to rover and base station, where the integer ambiguity resolution is estimated as part of the nonlinear observer state vector. The feedback interconnection of the observer systems is shown to be exponentially stable. The proposed observers are tested with an unmanned aerial vehicle simulator.**

I. Introduction

Vehicle navigation is often based on data from Inertial Measurement Units (IMUs) supplying inertial information such as acceleration and angular velocity of the vehicle. Integration of the measurements allows for estimation of position, linear velocity and attitude of the vehicle, which can be further enhanced by use of aiding sensors, e.g. a magnetometer or a Global Navigation Satellite System (GNSS) receiver.

One method for INS/GNSS integration is the loosely coupled architecture, where a kinematic model is used to integrate INS to position while correcting it with GNSS position data. Another approach is the tightly coupled architecture where range measurements from a GNSS system is used instead of position estimates for aiding. The primary difference between the loosely and tightly coupled systems is that the GNSS measurements are moved from the position-domain to the range-domain, see [1].

The accuracy of GNSS measurements suffer from signal disturbances e.g. in the ionosphere and troposphere where the signal path can be obstructed due to shifts in magnetic field or atmospheric density. These disturbances can, to some extend, be modeled based on local and solar weather forecasts. Using multi-frequency receivers it is possible to estimate and compensate for ionospheric delay, section 8.6 in [2], however these receivers are presently not widely used due to their high price. Another approach for countering the atmospheric disturbances is to utilize a dual receiver configuration, where two receivers are placed close to each other obtaining GNSS measurements from the same satellite constellation. In this case environmental disturbances are considered to be the same for the two receivers. With a known position of the reference receiver, often called base station, and a short baseline to the rover (vehicle) the signal disturbances can be canceled.

Using the raw measurements from the satellite receiver, i.e. carrier-phase, pseudo-range or Doppler frequency measurements, tight integration with the inertial measurements allow for an increase in precision, e.g. [1]. Multiple approaches for tight integration using Kalman filters have been proposed. Potential enhancements for tightly coupled integration on small unmanned aerial vehicles (UAVs) are listed in [3]. A Kalman filter method using GPS velocity estimates instead of carrier-phase measurements is proposed in [4]. An extended Kalman filter integrating pseudo-ranges and Doppler measurements with a low-cost inertial sensor is proposed in [5] for assisting the phase-lock-loop tracking. [6] use time-differenced carrier-phase measurements to eliminate the ambiguities. The time-differenced approach was also applied in [7] where an attitude determination system was designed using a Kalman filter and a single-receiver configuration. In [8] the advantages of augmenting precise point positioning with inertial measurements in a dual-frequency receiver configuration is investigated. The Kalman filter is based on linear approximation of the nonlinear measurement model, where a need for higher order accuracy was investigated in [9], but found to be negligible for tightly coupled systems. A comparative study of loosely, tightly and ultra-tightly coupled systems was investigated by [10] using a wide range of inertial sensor grades, and the GIGET tool. A tightly coupled system utilizing a GPS compass for effective integer ambiguity search was investigated by [11], using a low-cost multi-antenna setup. In [12] a new and faster method for integer ambiguity resolution is proposed, which is confirmed with experimental measurements.

Integration of inertial measurements and global position measurements have been researched extensively, traditionally in filters as the extended Kalman filter [1], [2], and recently with nonlinear observers [13], [14]. The advantages of the nonlinear observers compared to the widely used extended Kalman filter are the reduced computational workload, proven stability qualities and reduced need for linearization of the system model. An advantage of using raw satellite measurements is that the solution is no longer dependent of the unknown properties of the Kalman filter in the GNSS receiver supplying position estimates.

[1]Centre for Autonomous Marine Operations and Systems, Department of Engineering Cybernetics, Norwegian University of Science and Technology, 7491 Trondheim, Norway (e-mail: jakob.mahler.hansen@itk.ntnu.no, tor.arne.johansen@itk.ntnu.no, thor.fossen@ntnu.no)

978-1-4673-8681-4/$31.00 ©2016 AACC

The main contributions of the present paper are two nonlinear translational motion observers utilizing as injection the error between measured and estimated single- and double-differenced range measurements from the satellite constellation to rover and base station. For the single-differenced method the receiver clock error needs to be estimated, whereas this term is canceled for the double-differenced approach. Where various Kalman filters for tightly coupled integration have been put forward, and several nonlinear observers have been proposed for loosely coupled GNSS/INS integration, tight integration using nonlinear observers has only recently been proposed, [15] and [16], [17], [18], [19]. The motivation is reduced computational load and more transparent conditions for stability and region of attraction.

The problem will be stated formally in Section II, followed by the Real-Time-Kinematic (RTK) positioning approach in Section III, introducing the raw GNSS measurements. In Section IV and V the nonlinear observers will be introduced, while Section VI presents the method used for integer ambiguity resolution. In Section VII some implementation and time scale considerations are presented. A case study is conducted in Section VIII presenting data from a simulated unmanned aerial vehicle (UAV). The paper is concluded in Section IX.

II. Problem Statement

The objective of this paper is to estimate position, linear velocity and attitude (PVA) of a vehicle by tightly coupled integration of inertial measurements in the Body frame aided by range measurements from satellites. The satellite measurements include pseudo-range and carrier-phase measurements, obtained from the satellite broadcasts. The nonlinear observer is based on [15], with several extensions such that the position estimate is computed as a moving-baseline RTK solution with fixed or real valued integer ambiguities and known base station position. The raw satellite signal measurements are obtained at two locations: a stationary (or slightly moving) base station and a moving rover. Estimation of the rover PVA as well as the baseline, i.e. the vector (displacement) between rover and base station, are of interest. The coordinate frames used will be denoted with b for Body-frame and e for Earth-Centered-Earth-Fixed-frame. Here the rover and base station will be signified by the indicators r and s, respectively.

The kinematic model of the rover and base station are described by:

$$\dot{p}_r^e = v_r^e, \tag{1}$$
$$\dot{v}_r^e = -2S(\omega_{ie}^e)v_r^e + f^e + g^e(p_r^e), \tag{2}$$
$$\dot{q}_b^e = \frac{1}{2}q_b^e \otimes \bar{\omega}_{ib}^b - \frac{1}{2}\bar{\omega}_{ie}^e \otimes q_b^e, \tag{3}$$
$$\dot{b}^b = 0, \tag{4}$$
$$\dot{p}_s^e = 0, \tag{5}$$

where p_r^e, v_r^e and q_b^e denote the position, linear velocity and attitude of the rover, with the attitude represented as a unit quaternion expressed in the Earth-Centered-Earth-Fixed (ECEF) frame. The base station position, p_s^e, is assumed to be constant (or, in practice slowly time-varying). The specific force is denoted f^e, while the gravitational vector, g^e, is a function of the rover position. The angular velocity and associated rate gyro bias are denoted; ω_{ib}^b and b^b, expressed in the Body-frame, while the angular velocity of the Earth with respect to the Earth-Centered Inertial (ECI) frame is denoted ω_{ie}^e. The skew-symmetric matrix of a vector is denoted $S(\cdot)$ (see (B.14)–(B.15) [2]), while the Hamilton quaternion product is denoted $\otimes$. A real valued vector, $x \in \mathbb{R}^3$, can be expressed as a quaternion with zero real part denoted as $\bar{x} = [0; x]$.

A. Measurement Assumptions

Determining the position of a vehicle using RTK requires two receivers, separated by a baseline. The RTK principle is based on the assumption that the ionospheric and tropospheric disturbances for the two receivers are identical, thereby making it possible to cancel them out by sharing the obtained satellite data between the two receivers.

In the literature the carrier-phase measurements can be found with unit of meters or cycles. In the following φ will denote the carrier-phase measurement in meters, with $\varphi = \lambda\varphi_{cycles}$ being the conversion from cycles to meters, where λ is the wavelength of the signal.

The range measurements from the ith satellite are:

$$\rho_i^r = \psi_i^r + \beta^r + \varepsilon_i^r, \tag{6}$$
$$\varphi_i^r = \psi_i^r + N_i^r\lambda + \beta^r + e_i^r, \tag{7}$$

where ψ_i^r is the geometric range from the ith satellite to the rover, i.e. $\psi_i^r = \|p_r^e - p_i^e\|_2$. N_i^r is the integer ambiguity, β^r is the receiver clock range error, e_i^r and ε_i^r are covering systematic environmental errors arising from the ionosphere and troposphere. The receiver clock range error is expressed as, $\beta := c\Delta_c$, with c being the wave propagation speed and Δ_c being the clock bias, between satellite and receiver clocks. In addition, there are smaller errors such as receiver noise that is not explicitly included. When expressing the measurements at the base station the superscript r is substituted for s.

The environmental disturbances are the same for the base station and rover receiver, $e_i^r = e_i^s = e_i$ and $\varepsilon_i^r = \varepsilon_i^s = \varepsilon_i$, where the subscript denotes measurements from the ith satellite. Effectively this requires the baseline between the two antennas to be less than 20 km, [1].

The following sensor measurements are assumed available from the rover:

- Specific force as measured by an IMU, $f_{IMU}^b = f^b$.
- Angular velocity with bias as measured by an IMU, $\omega_{ib,IMU}^b = \omega_{ib}^b + b^b$.
- Magnetic field measurements from a magnetometer, m^b.
- Pseudo-ranges measurements from satellites, ρ_i^r.
- Carrier-phase measurements from satellites, φ_i^r.

Furthermore, it is assumed that pseudo-range, ρ_i^s, and carrier-phase, φ_i^s, measurements are available at the base station. There should be $m \geq 5$ common satellites available in the two constellations.

The satellite positions are assumed known, which can be satisfied by obtaining the transmitted ephemeris data from each satellite.

The method can be easily extended to exploit range-rate (Doppler) measurements, which are not included here for simplicity.

III. Real-Time-Kinematics Positioning

The single-differenced measurements between the rover and base station from the ith satellite can eliminate the common environmental errors:

$$\Delta\rho_i = \Delta\psi_i + \Delta\beta, \tag{8}$$
$$\Delta\varphi_i = \Delta\psi_i + \Delta N_i\lambda + \Delta\beta, \tag{9}$$

where $\Delta\rho_i := \rho_i^r - \rho_i^s$, $\Delta\varphi_i := \varphi_i^r - \varphi_i^s$, $\Delta N := N_i^r - N_i^s = [\Delta N_1, \Delta N_2, \ldots, \Delta N_m]$, $\Delta\beta := \beta^r - \beta^s$, and $\Delta\psi_i := \psi_i^r - \psi_i^s$ is the geometric baseline between rover and base station.

Elimination of the clock error $\Delta\beta$ can be achieved by double-differencing the measurements using an additional satellite j at the same epoch:

$$\nabla\Delta\rho_{ij} = \nabla\Delta\psi_{ij}, \tag{10}$$
$$\nabla\Delta\varphi_{ij} = \nabla\Delta\psi_{ij} + \nabla\Delta N_{ij}\lambda, \tag{11}$$

where $\nabla\Delta\rho_{ij} := \Delta\rho_j - \Delta\rho_i$, $\nabla\Delta\psi_{ij} := \Delta\psi_j - \Delta\psi_i$, $\nabla\Delta\varphi_{ij} := \Delta\varphi_j - \Delta\varphi_i$, and $\nabla\Delta N_{ij} := \Delta N_j - \Delta N_i$. It is vital that the measurements from the two satellites at the two receivers are simultaneous. If this is not the case the geometric distance between satellite and receiver will have changed between the measurements making the differential measurements inaccurate. The receivers are assumed to log and time stamp the raw measurements simultaneously for all satellites in the constellation with a fixed update rate of $1-10$ Hz. Moreover, it is assumed that coinciding measurements can be found for the two satellites at the two receivers.

In the following sections two nonlinear observers will be introduced, based on the single- and double-differenced measurements. The nonlinear observer design consists of two parts: an attitude observer and a translational motion observer.

IV. Nonlinear Observer - Single-Differenced

Estimating the rover attitude represented as the rotation between ECEF- and Body-frame as well as the gyro bias is achieved by the nonlinear attitude observer given in [20], [15], [21]:

$$\dot{\hat{q}}_b^e = \frac{1}{2}\hat{q}_b^e \otimes \left(\bar{\omega}_{ib,IMU}^b - \bar{\hat{b}}^b + \bar{\tilde{\sigma}}\right) - \frac{1}{2}\bar{\omega}_{ie}^e \otimes \hat{q}_b^e, \tag{12}$$
$$\dot{\hat{b}}^b = \mathrm{Proj}(-k_I\hat{\sigma}, \|\hat{b}^b\|_2 \leq M_{\hat{b}}), \tag{13}$$
$$\hat{\sigma} = k_1 v_1^b \times R(\hat{q}_b^e)^T v_1^e + k_2 v_2^b \times R(\hat{q}_b^e)^T v_2^e, \tag{14}$$

where $\mathrm{Proj}(\cdot,\cdot)$ is the projection function limiting the estimate to a sphere with constant radius $M_{\hat{b}}$. The magnetic field of the Earth is denoted m^e, while k_1, k_2 and k_I are positive constants chosen sufficiently large. The vectors v_1^b and v_2^b are two vectors in the Body-frame with corresponding vectors v_1^e and v_2^e in the ECEF-frame. The vectors can be considered in various forms, but will here be:

$$v_1^b = \frac{f_{IMU}^b}{\|f_{IMU}^b\|_2}, v_2^b = \frac{m^b}{\|m^b\|_2} \times v_1^b,$$
$$v_1^e = \frac{\hat{f}^e}{\|\hat{f}^e\|_2}, v_2^e = \frac{m^e}{\|m^e\|_2} \times v_1^e.$$

The specific force estimate is supplied by the translational motion observer, inspired by [15]:

$$\dot{\hat{p}}_r^e = \hat{v}_r^e + \sum_{i=1}^m \left(K_i^{p\rho} e_{\rho,i} + K_i^{p\varphi} e_{\varphi,i}\right), \tag{15}$$
$$\dot{\hat{v}}_r^e = -2S(\omega_{ie}^e)\hat{v}_r^e + \hat{f}^e + g^e(\hat{p}_r^e) + \sum_{i=1}^m \left(K_i^{v\rho} e_{\rho,i} + K_i^{v\varphi} e_{\varphi,i}\right), \tag{16}$$
$$\dot{\xi} = -R(\hat{q}_b^e)S(\hat{\sigma})f_{IMU}^b + \sum_{i=1}^m \left(K_i^{\xi\rho} e_{\rho,i} + K_i^{\xi\varphi} e_{\varphi,i}\right), \tag{17}$$
$$\hat{f}^e = R(\hat{q}_b^e)f_{IMU}^b + \xi, \tag{18}$$
$$\dot{\hat{p}}_s = \sum_{i=1}^m \left(K_i^{s\rho} e_{\rho,i} + K_i^{s\varphi} e_{\varphi,i}\right), \tag{19}$$
$$\Delta\dot{\hat{\beta}} = \sum_{i=1}^m \left(K_i^{\beta\rho} e_{\rho,i} + K_i^{\beta\varphi} e_{\varphi,i}\right), \tag{20}$$
$$\Delta\dot{\hat{N}} = \sum_{i=1}^m \left(K_i^{N\rho} e_{\rho,i} + K_i^{N\varphi} e_{\varphi,i}\right). \tag{21}$$

The clock error, $\Delta\beta$, is assumed to be the same for all satellites, i.e. $\Delta\hat{\beta} \in \mathbb{R}^1$. The receiver errors are assumed to dominate the clock range error diminishing the need for individual estimation for each satellite.

The single-differenced ambiguities, $\Delta\hat{N}$, are initially treated as real valued when estimated in (21), where Section VI will describe how the estimates are fixed to integer values for increased precision. The observer structure is similar to [15], with altered injection terms and addition of base station position and integer ambiguity estimation. The injection terms are the errors in single-differenced pseudo-range and carrier-phase, defined as: $e_{\rho,i} := \Delta\rho_i - \Delta\hat{\rho}_i$ and $e_{\varphi,i} := \Delta\varphi_i - \Delta\hat{\varphi}_i$. The estimated terms are determined as:

$$\Delta\hat{\rho}_i = \Delta\hat{\psi}_i + \Delta\hat{\beta}, \quad \Delta\hat{\varphi}_i = \Delta\hat{\psi}_i + \Delta\hat{N}_i\lambda + \Delta\hat{\beta}, \tag{22}$$

where the geometric range difference estimate is:

$$\Delta\hat{\psi}_i = \|\hat{p}_r^e - p_i^e\|_2 - \|\hat{p}_s^e - p_i^e\|_2.$$

The measurement errors can be expressed as:

$$e_{\rho,i} = \|p_r^e - p_i^e\|_2 - \|\hat{p}_r^e - p_i^e\|_2 - \|p_s^e - p_i^e\|_2 + \|\hat{p}_s^e - p_i^e\|_2 + \Delta\tilde{\beta}, \tag{23}$$
$$e_{\varphi,i} = e_{\rho,i} + \Delta\tilde{N}_i\lambda. \tag{24}$$

The state estimation error vector is introduced as, $\tilde{x} = [\tilde{p}_r, \tilde{v}_r, \tilde{f}, \tilde{p}_s, \Delta\tilde{\beta}, \Delta\tilde{N}]^T$, with $\tilde{p}_r := p_r^e - \hat{p}_r^e$, $\tilde{v}_r := v_r^e - \hat{v}_r^e$, $\tilde{f} := f^e - \hat{f}^e$, $\tilde{p}_s := p_s^e - \hat{p}_s^e$, $\Delta\tilde{\beta} := \Delta\beta - \Delta\hat{\beta}$, $\Delta\tilde{N} := \Delta N - \Delta\hat{N}$, where ξ is replaced with $\tilde{f}$ by combination of (17) and (18). The measurement errors are linearized leaving:

$$e_{\rho,i} = C_{\rho,i}\tilde{x} + h.o.t., \tag{25}$$
$$e_{\varphi,i} = C_{\varphi,i}\tilde{x} + h.o.t., \tag{26}$$

where the higher order terms (*h.o.t.*) are neglected in the observer gain selection, [15]. The measurement matrices are given by their rows $C_{\rho,i} = [\underline{c}_i, 0, 0, \check{c}_i, 1, 0_m]$, and $C_{\varphi,i} = [\underline{c}_i, 0, 0, \check{c}_i, 1, \lambda 1_{i,m}]$ for $i = 1, 2, \ldots, m$, with $1_{i,m} = [0, \ldots, 1, \ldots, 0]$ having a non-zero ith element, and $\underline{c}_i$ and $\check{c}_i$ defined in Appendix A:

$$\underline{c}_i = \frac{\hat{p}_r^e - p_i^e}{\|\hat{p}_r^e - p_i^e\|_2}, \quad \check{c}_i = -\frac{\hat{p}_s^e - p_i^e}{\|\hat{p}_s^e - p_i^e\|_2}, \tag{27}$$

The error dynamics can be expressed as, [14], [15]:

$$\dot{\tilde{x}} = (A - KC)\tilde{x} + \theta_1(t, \tilde{x}) + \theta_2(t, \chi) + \theta_3(t, \tilde{x}), \tag{28}$$

where $\theta_1(t, \tilde{x}) := [0, \theta_{12}(t, \tilde{x}), 0, 0, 0]$ with $\theta_{12}(t, \tilde{x}) = -S(\omega_{ie}^e)\tilde{x}_2 + (g^e(p_r^e) - g^e(p_r^e - \tilde{x}_1))$ and $\theta_2(t, \chi)$ as given in [14] where it was shown that $\|\theta_2(t, \chi)\|_2 \leq \gamma_3 \|\chi\|_2$ for some positive constant γ_3. Here χ is the combined variable $\chi := [r; b]$ consisting of the vector part of the quaternion, r, and the gyro bias. The last term in (28) is defined as $\theta_3(t, \tilde{x}) = \lambda K[0; \Delta\tilde{N}] + h.o.t.$. The time-varying observer gains of the translational motion observer, K_i^*, must satisfy $A - KC$ being stable where:

$$A = \begin{bmatrix} 0 & I_3 & 0 & 0 & 0 & 0 \\ 0 & 0 & I_3 & 0 & 0 & 0 \\ 0 & 0 & 0 & 0 & 0 & 0 \\ 0 & 0 & 0 & 0 & 0 & 0 \\ 0 & 0 & 0 & 0 & 0 & 0 \\ 0 & 0 & 0 & 0 & 0 & 0 \end{bmatrix}, K = \begin{bmatrix} K_1^{p\rho} & \ldots & K_m^{p\rho} & K_1^{p\varphi} & \ldots & K_m^{p\varphi} \\ K_1^{v\rho} & \ldots & K_m^{v\rho} & K_1^{v\varphi} & \ldots & K_m^{v\varphi} \\ K_1^{\xi\rho} & \ldots & K_m^{\xi\rho} & K_1^{\xi\varphi} & \ldots & K_m^{\xi\varphi} \\ K_1^{s\rho} & \ldots & K_m^{s\rho} & K_1^{s\varphi} & \ldots & K_m^{s\varphi} \\ K_1^{\beta\rho} & \ldots & K_m^{\beta\rho} & K_1^{\beta\varphi} & \ldots & K_m^{\beta\varphi} \\ K_1^{N\rho} & \ldots & K_m^{N\rho} & K_1^{N\varphi} & \ldots & K_m^{N\varphi} \end{bmatrix}$$

and C is a time-varying matrix with $2m$ rows; $C := [C_{\rho,1}; \ldots; C_{\rho,m}; C_{\varphi,1}; \ldots; C_{\varphi,m}]$. It should be noted that the constellation and number of available satellites can change with every epoch.

Observability of the system (28) is ensured with a sufficient number of satellites, and the vectors v_1^e and v_2^e not being co-linear. An accurate initialization procedure is proposed in [15]. As shown in [15] this leads to exponential stability with semi-global region of attraction with respect to attitude initialization error when K is the gain matrix and P the covariance matrix determined by solving the time-varying Riccati equation, see Section VII.

V. Nonlinear Observer - Double-Differenced

An alternative observer is proposed based on the same observer structure as the single-differenced observer in Section IV, using double-differenced measurements. One advantage is that the estimation of the clock error is no longer required, making the state vector smaller compared to the single-differenced observer. With the attitude observer described by (12)–(14) as before, the double-differenced translational motion observer is proposed as:

$$\dot{\hat{p}}_r^e = \hat{v}_r^e + \sum_{j=1}^{m-1} \left(K_j^{p\rho} e_{\rho,mj} + K_j^{p\varphi} e_{\varphi,mj} \right), \tag{29}$$

$$\dot{\hat{v}}_r^e = -2S(\omega_{ie}^e)\hat{v}_r^e + \hat{f}^e + g^e(\hat{p}_r^e) + \sum_{j=1}^{m-1} \left(K_j^{v\rho} e_{\rho,mj} + K_j^{v\varphi} e_{\varphi,mj} \right), \tag{30}$$

$$\dot{\hat{\xi}} = -R(\hat{q}_b^e)S(\hat{\sigma})f_{IMU}^b + \sum_{j=1}^{m-1} \left(K_j^{\xi\rho} e_{\rho,mj} + K_j^{\xi\varphi} e_{\varphi,mj} \right), \tag{31}$$

$$\hat{f}^e = R(\hat{q}_b^e)f_{IMU}^b + \xi, \tag{32}$$

$$\dot{\hat{p}}_s^e = \sum_{j=1}^{m-1} \left(K_j^{s\rho} e_{\rho,mj} + K_j^{s\varphi} e_{\varphi,mj} \right), \tag{33}$$

$$\nabla\Delta\dot{\hat{N}} = \sum_{j=1}^{m-1} \left(K_j^{Np} e_{\rho,mj} + K_j^{N\varphi} e_{\phi,mj} \right). \tag{34}$$

The double-differenced integer ambiguities comprises a vector one element smaller than the single-differenced ambiguity vector, and will initially be treated as real valued, i.e. $\nabla\Delta\hat{N} \in \mathbb{R}^{m-1}$. The injection terms are the errors in double-differenced pseudo-range and carrier-phase, defined as: $e_{\rho,mj} := \nabla\Delta\rho_{mj} - \nabla\Delta\hat{\rho}_{mj}$ and $e_{\varphi,mj} := \nabla\Delta\varphi_{mj} - \nabla\Delta\hat{\varphi}_{mj}$. The estimated terms are determined as:

$$\nabla\Delta\hat{\rho}_{mj} = \nabla\Delta\hat{\psi}_{mj}, \quad \nabla\Delta\hat{\varphi}_{mj} = \nabla\Delta\hat{\psi}_{mj} + \nabla\Delta\hat{N}_{mj}\lambda, \tag{35}$$

with the double-differenced geometric range, $\nabla\Delta\hat{\psi}_{mj}$, being:

$$\nabla\Delta\hat{\psi}_{mj} = \|\hat{p}_r^e - p_j^e\|_2 - \|\hat{p}_r^e - p_m^e\|_2 - \|\hat{p}_s^e - p_j^e\|_2 + \|\hat{p}_s^e - p_m^e\|_2.$$

The injection terms can be expressed as:

$$e_{\rho,mj} = \|p_r^e - p_j^e\|_2 - \|p_r^e - p_m^e\|_2 - \|p_s^e - p_j^e\|_2 + \|p_s^e - p_m^e\|_2 - \|\hat{p}_r^e - p_j^e\|_2 + \|\hat{p}_r^e - p_m^e\|_2 + \|\hat{p}_s^e - p_j^e\|_2 - \|\hat{p}_s^e - p_m^e\|_2,$$

$$e_{\varphi,mj} = e_{\rho,mj} + \nabla\Delta\tilde{N}_{mj}\lambda.$$

Defining the state vector $\tilde{x} := [\tilde{p}_r, \tilde{v}_r, \tilde{f}, \tilde{p}_s, \nabla\Delta\tilde{N}]^T$, with $\nabla\Delta\tilde{N}_{mj} := \nabla\Delta N_{mj} - \nabla\Delta\hat{N}_{mj}$ and state substitution as for the single-differenced observer. The linearized measurement errors are:

$$e_{\rho,mj} = C_{\rho,mj}\tilde{x} + h.o.t., \tag{36}$$

$$e_{\varphi,mj} = C_{\varphi,mj}\tilde{x} + h.o.t., \tag{37}$$

where $C_{\rho,mj} = [\underline{c}_{mj}, 0, 0, \check{c}_{mj}, 0]$ and $C_{\varphi,mj} = [\underline{c}_{mj}, 0, 0, \check{c}_{mj}, \lambda 1_{j,m-1}]$, see Appendix B:

$$\underline{c}_{mj} = \frac{\hat{p}_r^e - p_j^e}{\|\hat{p}_r^e - p_j^e\|_2} - \frac{\hat{p}_r^e - p_m^e}{\|\hat{p}_r^e - p_m^e\|_2},$$

$$\check{c}_{mj} = -\frac{\hat{p}_s^e - p_j^e}{\|\hat{p}_s^e - p_j^e\|_2} + \frac{\hat{p}_s^e - p_m^e}{\|\hat{p}_s^e - p_m^e\|_2}.$$

The error dynamics for the double-differenced approach is:

$$\dot{\tilde{x}} = (A - KC)\tilde{x} + \theta_1(t, \tilde{x}) + \theta_2(t, \chi) + \theta_3(t, \tilde{x}), \tag{38}$$

where the perturbation terms are defined as for the single-differenced case, with the exclusion of the rows for the $\Delta\tilde{\beta}$ state. The time-varying observer gains of the translational motion observer, K_j^*, must satisfy $A - KC$ being stable where:

$$A = \begin{bmatrix} 0 & I_3 & 0 & 0 & 0 \\ 0 & 0 & I_3 & 0 & 0 \\ 0 & 0 & 0 & 0 & 0 \\ 0 & 0 & 0 & 0 & 0 \\ 0 & 0 & 0 & 0 & 0 \end{bmatrix}, K = \begin{bmatrix} K_1^{p\rho} & \ldots & K_{m-1}^{p\rho} & K_1^{p\varphi} & \ldots & K_{m-1}^{p\varphi} \\ K_1^{v\rho} & \ldots & K_{m-1}^{v\rho} & K_1^{v\varphi} & \ldots & K_{m-1}^{v\varphi} \\ K_1^{\xi\rho} & \ldots & K_{m-1}^{\xi\rho} & K_1^{\xi\varphi} & \ldots & K_{m-1}^{\xi\varphi} \\ K_1^{s\rho} & \ldots & K_{m-1}^{s\rho} & K_1^{s\varphi} & \ldots & K_{m-1}^{s\varphi} \\ K_1^{N\rho} & \ldots & K_{m-1}^{N\rho} & K_1^{N\varphi} & \ldots & K_{m-1}^{N\varphi} \end{bmatrix}$$

and C is a time-varying matrix with $2m-2$ rows; $C := [C_{\rho,m,1}; \ldots; C_{\rho,m,m-1}; C_{\varphi,m,1}; \ldots; C_{\varphi,m,m-1}]$. The gain and covariance matrix are found from the time-varying Riccati equation, see Section VII. Following the results of [15] the equilibrium point of the observer is exponentially stable with

a semi-global region of attraction with respect to attitude initialization error. The observer can be initialized with the procedure proposed in [15].

VI. Integer Ambiguity

The two proposed observers treat the ambiguity estimates as real valued, $\Delta\hat{N}_i$ and $\nabla\Delta\hat{N}_{ij}$, which can be improved upon by fixing the ambiguities to integers. Fixing the ambiguities can be done in several ways, here the focus will be on the "Fix and hold" method, [1].

The ambiguity resolution approach requires at least five satellites to be tracked simultaneous by the rover and base station, i.e. $m \geq 5$. The ambiguities are considered as a combined variable, e.g. $\Delta\hat{N} := \left[\Delta\hat{N}_1; \Delta\hat{N}_2; \ldots; \Delta\hat{N}_m\right]$ expressing the ambiguity vector.

The initial ambiguity vector estimates for the single- and double-differenced observers can be determined from subtraction of (8)–(9) and (10)–(11):

$$\Delta\hat{N} = \frac{1}{\lambda}\left(\Delta\varphi - \Delta\rho\right), \tag{39a}$$

$$\nabla\Delta\hat{N} = \frac{1}{\lambda}\left(\nabla\Delta\varphi - \nabla\Delta\rho\right), \tag{39b}$$

where $\Delta\varphi$, $\Delta\rho$, $\nabla\Delta\varphi$ and $\nabla\Delta\rho$ are combined variables of the single- and double-differenced range measurements.

These equations can be used for estimating the ambiguities by averaging over the differences for each epoch over a period of time. The drawback is extended initial computation time for ambiguity estimation. Here (39) will be used as an initial estimate of the ambiguities, determined for every new satellite in the constellation. The initialization should also be used if a satellite is re-introduced to the constellation after a period of blockage or loss of lock.

The observer will estimate the real-valued ambiguities as part of the state vector, updating the estimates with every epoch. The real valued estimates can then be tested for convergence to an integer value by searching through integer sets to minimize, [1] (here shown for the double-differenced observer):

$$s_N^2 = \left(\nabla\Delta\bar{N} - \nabla\Delta\hat{N}\right)^T P_N^{-1}\left(\nabla\Delta\bar{N} - \nabla\Delta\hat{N}\right), \tag{40}$$

where $\nabla\Delta\bar{N}$ is a vector of candidate integer values, and the ambiguity error covariance matrix is denoted $P_N > 0$. The search space of the integers, $\nabla\Delta\bar{N}$, is determined as:

$$S := \left\{\nabla\Delta\bar{N} \in \mathbb{Z}^{m-1} \middle| \nabla\Delta\hat{N} - c_r\sigma_N \leq \nabla\Delta\bar{N} \leq \nabla\Delta\hat{N} + c_r\sigma_N\right\},$$

where σ_N is the variance of the integer estimates determined as the square root of the diagonal elements of P_N, i.e. $\sigma_N = \sqrt{\mathrm{diag}(P_N)}$. The constant c_r denotes the size of the confidence interval, where in the following, assuming normal distribution, $c_r := 3.29$ for 99.9% confidence interval.

After evaluation of (40) the smallest and second smallest value of $s_{N,i}^2$, respectively called Ω_1 and Ω_2 are used to test if a candidate set is sufficiently close to the estimated ambiguities. This is done by testing whether Ω_1 is far enough from other solutions to make it stand out:

$$\Omega_2\Omega_1^{-1} \geq t_N$$

If the ratio is greater than some threshold, the test is accepted and the integer candidate corresponding to Ω_1 is chosen as the fixed ambiguity estimate, $\nabla\Delta\check{N} := \left[\nabla\Delta\check{N}_{m,1}; \nabla\Delta\check{N}_{m,2}; \ldots; \nabla\Delta\check{N}_{m,m-1}\right]$. This test is performed for every epoch and will use all the present ambiguities in the decision. It is therefore not possible to fit part of the ambiguity vector to integer value and leaving some as real-valued.

Since the search space for the integer ambiguity resolution initially will be too large to be computationally feasible, the integer evaluation will only be carried out when the search space is smaller than some limit, e.g. 100 000 possibilities, which is determined by σ_N.

VII. Implementation Considerations

The translational motion observers are discretized using the Corrector-Predictor method presented in [22], where the observer is divided into a linear corrector part consisting of the injection terms and a nonlinear predictor part. The predictor part is implemented at IMU sampling frequency predicting the states between satellite measurements, which updates the slower corrector part. The attitude observer is implemented at IMU sampling frequency using Euler integration.

The implementation is divided into three time-scales:

- IMU: The attitude observer and the predictor part of the translational motion observer are implemented at IMU frequency, becoming the fastest time scale.
- GNSS: The corrector part of the translational motion observer is driven by the frequency of raw measurements from the satellites. Estimation of the satellite positions have to be available for every iteration of the raw measurements. These can be estimated using the broadcasted ephemeris data.
- Gains: The line-of-sight vectors of the satellites are slowly time-varying and the gain matrix K of the translational motion observer can therefore be updated on the slowest time scale. To save computational effort the observer gains can be determined every few minutes instead of at GNSS receiver frequency, [15].

The gain matrices and covariance matrix, can be determined by solving the discrete time-varying Riccati equation:

$$P_{k|k-1} = A_d P_{k-1|k-1} A_d^T + Q^T, \tag{41}$$

$$K_k = P_{k|k-1} C^T \left(C P_{k|k-1} C^T + R\right)^{-1}, \tag{42}$$

$$P_{k|k} = \left(I_n - K_k C\right) P_{k|k-1} \left(I_n - K_k C\right) + K_k R K_k^T, \tag{43}$$

where A_d is the discretized A matrix, using sample rate equal to the GNSS frequency. The system order is denoted n. The state and measurement covariance matrices are denoted $Q > 0$ and $R > 0$. The R matrix consists of diagonal elements of the range noise variance. The observer is tuned using the parameters in Q, which describes the anticipated variance of the process noise. The elements corresponding to position and linear velocity in Q matrix are often beneficial to keep small to obtain smooth estimates, whereas the specific force element can be chosen larger. It is vital that the element corresponding to the clock bias is chosen sufficiently large such that the estimates can converge fast.

The covariance matrix of the ambiguities, P_N, is the submatrix of the state covariance matrix, P, found as the $(m-1)\times(m-1)$ lower right part of P (or $m\times m$ for the single-differenced observer).

VIII. Simulation Example

A simulation study is carried out to compare the performance of the two proposed translational motion observers. The UAV simulator presented in [23] is used with an Aerosonde type UAV.

The differenced pseudo-range and carrier-phase measurements are created from (8) and (9) at a frequency of 5 Hz, with added noise. The noise is a first order Markov process, with time constant of 60 s, where white noise with standard deviation of 5 m is low-pass filtered into pseudo-range and carrier-phase measurement noise. The rover and base station measurements experiences the same Markov noise to simulate the same ionosphere and troposphere. An additional, smaller white noise have been added to the rover measurements, with variances of 0.10 m and 0.001 m, to simulate receiver noise on pseudo-range and carrier-phase measurements. The geometric distance $\Delta\psi_i$ is computed using the known satellite and receiver positions given in Table I.

In the simulations the satellite velocities will be assumed constant, making the satellite paths linear instead of curved, which is a realistic condition only for a short period of time but keeps the simulation simple. A scenario consisting of a stationary base station and the UAV moving in a counter-clockwise motion in the local xy-plane with a radius of 650 m is simulated.

The accelerometer, magnetometer and gyroscope measurements are simulated with a frequency of 400 Hz, where white noise have been added with standard deviations of 0.0015 m/s^2, 0.45 $mGauss$, and 0.16 deg/s, corresponding to the noise specification similar to an Analog Devices 16488 IMU.

The observer gains are determined by solving a discrete Riccati equation using the matrices given in Sections IV and V, and $R = \text{blkdiag}(0.10I_m, 0.001I_m)$ and $Q = \text{blkdiag}(0I_3, 10^{-5}I_3, 2.5\cdot10^{-3}I_3, 0I_3, 1000, 10^{-2}I_m)$, where the 13th element is only used in the single-differenced observer. Furthermore, $M_b = 0.0087$, $k_1 = 0.8$, $k_2 = 0.2$, $k_I = 0.004$, and $\lambda = 0.1903$ m. The single-differenced observer is sensitive towards the initial value of $\Delta\hat{\beta}$ and therefore needs a good initial estimate, which can be found as; $\Delta\hat{\beta}_0 \approx \Delta\rho_0 = \rho^r_{i,0} - \rho^s_{i,0}$, being the initial pseudo-range difference measurement.

The estimation errors with real valued and fixed ambiguities are depicted in Fig. 1, for single-difference, and Fig. 2 for double-differenced.

Within 10 seconds the errors are smaller than 10cm. However a small stationary error is present due to measurement noise. The performance of the four observers are comparable, where the double-differenced observer has a better base station estimate. The sinusoidal effect on the rover estimates is caused by the chosen flight path. To showcase the expected

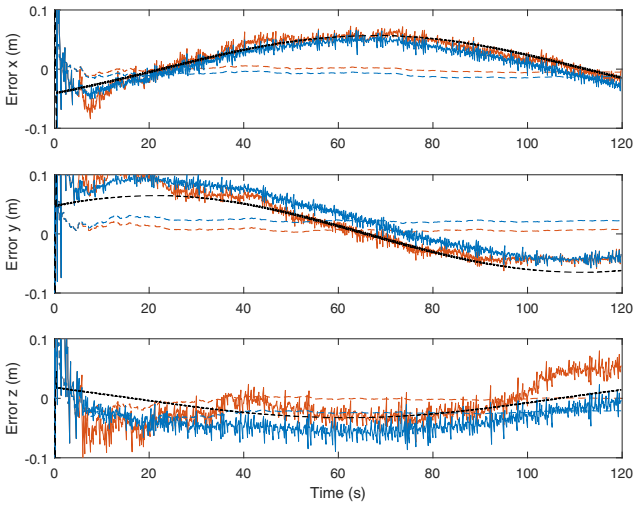

Fig. 1. Position errors of single-difference observer with real valued (red) and fixed ambiguities (blue). Base station error in dashed lines and rover error in solid lines. The noise free simulation is shown with black dashed lines.

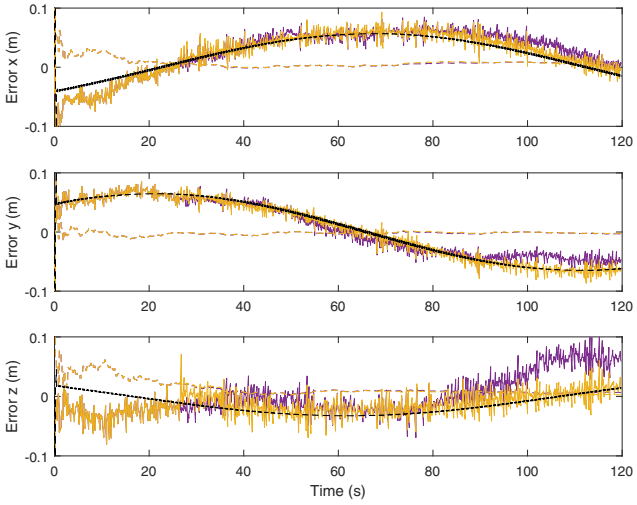

Fig. 2. Position errors of double-difference observer with real valued (magenta) and fixed ambiguities (yellow). Base station error in dashed lines and rover error in solid lines. The noise free simulation is shown with black dashed lines.

effect a case without any noise is included in Fig. 1 and Fig. 2 as black lines. It is evident that the observers with fixed integers follow the sinusoidal effect best. No such effect is present during a straight flight path.

As an example of the real valued ambiguity errors, the estimation of ΔN_{11} and $\nabla\Delta N_{1,11}$ is depicted in Fig. 3. Similar behavior is seen for the other satellites.

The ambiguities are fixed before 30s. The small difference between the four observer estimates is due to the real valued ambiguities being close to the true fixed value.

IX. Conclusions

Two nonlinear translational motion observers were proposed for estimating position, linear velocity and attitude using tightly coupled INS/GNSS integration in a dual GNSS-

TABLE I

SATELLITE POSITIONS, VELOCITIES AND INTEGER AMBIGUITIES

SV	x (m)	y (m)	z (m)	$\dot{x}$ (m/s)	$\dot{y}$ (m/s)	$\dot{z}$ (m/s)	ΔN_i $(-)$	$\nabla\Delta N_{1j}$ $(-)$
1	18590267.86	6297568.79	17915716.72	1066.87	2019.92	-1796.36	600800	-
11	23052191.14	9482190.19	8876630.61	654.73	1108.85	-2708.86	-1937600	2538400
14	-8320592.86	14161791.19	21076475.35	-2618.08	-183.57	-934.84	-703500	1304300
17	9289670.11	-14108222.35	20708751.43	2571.02	114.34	-1112.15	267900	332900
20	17875487.82	-5874206.28	18521323.27	-807.28	2276.52	1492.19	-873800	1474600
31	4341972.44	23303879.02	11796460.36	-931.45	-1174.28	2728.45	338600	262200
32	11724367.18	10345207.31	21515170.95	-1480.32	2293.47	-241.92	-1007600	1608400

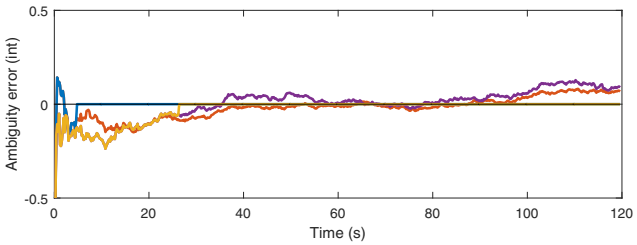

Fig. 3. Estimation error of real valued integer ambiguity in single- (red) and double- (magenta) differenced observer, with the fixed ambiguities of the single- (blue) and double- (yellow) differenced observers.

receiver environment. The position of a moving rover and a stationary base station are estimated as states of the observers. The observers utilize the error between measured and estimated range from satellite constellation to the rover and base station.

The difference between the proposed observers is the range measurement model. The first observer uses the single-differenced approach, where the clock range error is also included in the state vector, while the second observer utilize the double-differenced measurements. In both cases the integer ambiguity of the carrier-phase measurements are resolved.

The observers are verified using a UAV simulator, showing convergence of integer ambiguity as well as small estimation errors for position of rover and base station.

APPENDIX

A. Single-Differenced Injection Terms

Inspired by [15] the measurement errors are expanded as a second order Taylor's polynomial. First lets consider the base station terms of the measurement error in (23):

$$e_{\rho,i,s} = \|p_s^e - p_i^e\|_2 - \|\hat{p}_s^e - p_i^e\|_2. \tag{44}$$

The Taylor approximation of $h(p_s^e) := \|p_s^e - p_i^e\|_2$ at a point $\hat{p}_s^e = p_s^e$ is then:

$$h(p_s^e) \approx \|\hat{p}_s^e - p_i^e\|_2 + \left(\frac{\hat{p}_s^e - p_i^e}{\|\hat{p}_s^e - p_i^e\|_2}\right)^T (\hat{p}_s^e - p_s^e) + h.o.t.$$

$$e_{\rho,i,s} \approx \left(\frac{\hat{p}_s^e - p_i^e}{\|\hat{p}_s^e - p_i^e\|_2}\right)^T \tilde{p}_s^e + h.o.t.$$

Following the same approach the Taylor approximation for the rover term can be found. Only $e_{\rho,i}$ will be shown as $e_{\varphi,i}$ follows directly from this:

$$\begin{aligned} e_{\rho,i} = &\left(\frac{\hat{p}_r^e - p_i^e}{\hat{\psi}_i}\right)^T \tilde{p}_r + \left(\frac{\hat{p}_s^e - p_i^e}{\hat{\psi}_{s,i}}\right)^T \tilde{p}_s^e + \Delta\tilde{\beta} \\ &+ \frac{1}{2}\tilde{p}_r^T \check{H}_i \tilde{p}_r + \frac{1}{2}\tilde{p}_s^T \check{H}_{s,i} \tilde{p}_s, \end{aligned} \tag{45}$$

with

$$\check{H}_i = \frac{1}{\check{\psi}_i} I_3 - \frac{(\check{p}_r^e - p_i^e)(\check{p}_r^e - p_i^e)^T}{\check{\psi}_i^3}. \tag{46}$$

$$\check{H}_{s,i} = \frac{1}{\check{\psi}_{s,i}} I_3 - \frac{(\check{p}_s^e - p_i^e)(\check{p}_s^e - p_i^e)^T}{\check{\psi}_{s,i}^3}. \tag{47}$$

The higher order term considers a point $\check{p}_r^e$ on the line between the estimated and true rover position, with corresponding satellite distance $\check{\psi}_i = \|\check{p}_r^e - p_i^e\|_2$. Similarly is $\check{p}_s^e$ defined as a point between estimated and true base station position with $\check{\psi}_{s,i} = \|\check{p}_s^e - p_i^e\|_2$. Bounds on the last terms of (45), $\gamma_i = 1/2\tilde{p}^T \check{H}_i \tilde{p}$ and $\gamma_{s,i} = 1/2\tilde{p}_s^T \check{H}_{s,i}\tilde{p}_s$, follows directly from [15]:

$$\|\gamma_i\|_2 \leq \frac{1}{\underline{\psi}}\|\tilde{p}_r\|_2^2, \quad \|\gamma_{s,i}\|_2 \leq \frac{1}{\underline{\psi}_s}\|\tilde{p}_s\|_2^2 \tag{48}$$

where $\underline{\psi}$ and $\underline{\psi}_s$ are assumed positive lower bounds on the geometric distances.

B. Double-Differenced Injection Terms

With Taylor's theorem by inspiration from [15] the measurement error can be written as:

$$\begin{aligned} e_{\rho,ij} = &\left(\frac{\hat{p}_r^e - p_j^e}{\hat{\psi}_j}\right)^T \tilde{p}_r - \left(\frac{\hat{p}_r^e - p_i^e}{\hat{\psi}_i}\right)^T \tilde{p}_r + \frac{1}{2}\tilde{p}_r^T \left(\check{H}_j - \check{H}_i\right)\tilde{p}_r \\ &+ \left(\frac{\hat{p}_s^e - p_j^e}{\hat{\psi}_{s,j}}\right)^T \tilde{p}_s - \left(\frac{\hat{p}_s^e - p_i^e}{\hat{\psi}_{s,i}}\right)^T \tilde{p}_s + \frac{1}{2}\tilde{p}_s^T \left(\check{H}_{s,j} - \check{H}_{s,i}\right)\tilde{p}_s \end{aligned}$$

with $\check{H}_i$ and $\check{H}_{s,i}$ given by (46)–(47). The expression for $\check{H}_j$ and $\check{H}_{s,j}$ are found from (46)–(47) by substituting i with j.

The higher order terms are bounded similarly to the single-differenced observer:

$$\gamma_j = \frac{1}{2}\tilde{p}_r^T \left(\check{H}_j - \check{H}_i\right)\tilde{p}_r, \qquad \|\gamma_j\|_2 \leq \frac{2}{\underline{\psi}}\|\tilde{p}_r\|_2^2, \tag{49}$$

$$\gamma_{s,j} = \frac{1}{2}\tilde{p}_s^T \left(\check{H}_{s,j} - \check{H}_{s,i}\right)\tilde{p}_s, \qquad \|\gamma_{s,j}\|_2 \leq \frac{2}{\underline{\psi}_s}\|\tilde{p}_s\|_2^2, \tag{50}$$

where the geometric distances from the rover and base station to the ith and jth satellite are both assumed to be lower bounded by $\underline{\psi}$ and $\underline{\psi}_s$, respectively.

ACKNOWLEDGMENT

This work was supported by the Norwegian Research Council (projects no. 221666 and 223254) through the Centre of Autonomous Marine Operations and Systems at the Norwegian University of Science and Technology. The authors would like to thank Nadezda Sokolova, SINTEF.

REFERENCES

[1] P. D. Groves, *Principles of GNSS, Inertial, and Multisensor Integrated Navigation Systems*. Artech House, 2013.

[2] J. A. Farrell, *Aided Navigation: GPS with High Rate Sensors*. McGraw Hill, 2008.

[3] M. George and S. Sukkarieh, "Tightly Coupled INS/GPS With Bias Estimation for UAV Application," *Proceedings of Australiasian Conference on Robotics and Automation (ACRA)*, vol. -, pp. –, 2005.

[4] S. Moafipoor, D. A. Grejner-Brzezinska, and C. K. Toth, "Tightly Coupled GPS/INS Integration Based on GPS Carrier Phase Velocity Update," *ION NTM*, vol. -, pp. –, 2004.

[5] Y. Tawk, P. Tomé, C. Botteron, Y. Stebler, and P.-A. Farine, "Implementation and Performance of a GPS/INS Tightly Coupled Assisted PLL Architecture Using MEMS Inertial Sensors," *Sensors*, vol. 14, pp. 3768–3796, 2014.

[6] Y. Zhao, M. Becker, D. Becker, and S. Leinen, "Improving the Performance of Tightly-Coupled GPS/INS Navigation by Using Time-Differenced GPS-Carrier-Phase Measurements and Low-Cost MEMS IMU," *ISSN, Gyroscopy and Navigation*, vol. 6, 2, pp. 133–142, 2015.

[7] J. Wendel, T. Obert, and G. F. Trommer, "Enhancement of a Tightly Coupled GPS/INS System for High Precision Attitude Determination of Land Vehicle," *Proceedings ION 59th AM*, pp. 20–208, 2003.

[8] R. M. Watson, V. Sivaneri, and J. N. Gross, "Performance Characterization of Tightly-Coupled GNSS Precise Point Positioning Inertial Navigation wiwith a Simulation Environment," *AIAA Guidance, Navigation, and Control Conference*, pp. 1–18, 2016.

[9] J. Wendel, J. Metzger, R. Moenikes, A. Maier, and G. F. Trommer, "A Performance Comparison of Tightly Coupled GPS/INS Navigation Systems based on Extended and Sigma Point Kalman Filters," *Navigation: JION*, vol. Vol. 53, No. 1, pp. 21–31, 2006.

[10] J. D. Gautier and B. W. Parkinson, "Using the GPS/INS Generalized Evaluation Tool (GIGET) for the Comparison of Loosely Coupled, Tightly Coupled and Ultra-Tightly Coupled Integrated Navigation Systems," *Proc. ION CIGTF*, pp. 65–76, 2003.

[11] R. Hirokawa and T. Ebinuma, "A Low-Cost Tightly Coupled GPS/INS for Small UAVs Augmented with Multiple GPS Antennas," *Navigation: JION*, vol. Vol. 56, No. 1, pp. 35–44, 2009.

[12] Y. Chen, S. Zhao, and J. A. Farrell, "Computationally Efficient Carrier Integer Ambiguity Resolution in Multiepoch GPS/INS: A Common-Position-Shift Approach," *IEEE Transactions on Control Systems Technology*, pp. 1–16, 2015.

[13] M.-D. Hua, "Attitude Estimation for Accelerated Vehicles using GPS/INS Measurements," *Control Engineering Practice*, vol. 18, pp. 723–732, 2010.

[14] H. F. Grip, T. I. Fossen, T. A. Johansen, and A. Saberi, "Nonlinear Observer for GNSS-Aided Inertial Navigation with Quaternion-Based Attitude Estimation," *American Control Conference*, vol. -, pp. 272–279, 2013.

[15] T. A. Johansen and T. I. Fossen, "Nonlinear Observer for Inertial Navigation Aided by Pseudo-Range and Range-Rate Measurements," *European Control Conference*, vol. -, pp. –, 2015.

[16] P. Batista, "Long Baseline Navigation With Clock Offset Estimation and Discrete-Time Measurements," *Control Engineering Practice*, vol. 35, pp. 43–53, 2015.

[17] P. Batista, "GES Long Baseline Navigation With Unkown Sound Velocity and Discrete-Time Range Measurements," *IEEE Transactions on Control Systems Technology*, vol. 23, pp. 219–230, 2015.

[18] P. Batista, C. Silvestre, and P. Oliveira, "Single Range Aided Navigation and Source LocalizLocal: Observability and Filter Design," *Systems and Control Letters*, vol. 60, pp. 665–673, 2011.

[19] P. Batista, C. Silvestre, and P. Oliveira, "Tightly Coupled Long Baseline/Ultra-Short Baseline Integrated Navigation System," *International Journal of Systems Science*, pp. 1–19, 2014.

[20] R. Mahony, T. Hamel, and J.-M. Pflimlin, "Nonlinear Complementary Filters on the Special Orthogonal Group," *IEEE Transactions on Automatic Control*, vol. 53, No 5, pp. 1203–1218, 2008.

[21] H. F. Grip, T. I. Fossen, T. A. Johansen, and A. Saberi, "Attitude Estimation Using Biased Gyro and Vector Measurements With Time-Varying Reference Vectors," *IEEE Transactions on Automatic Control*, vol. 57, pp. 1332–1338, 2012.

[22] T. I. Fossen, *Handbook of Marine Craft Hydrodynamics and Motion Control*. John Wiley & Sons, Ltd, 2011.

[23] R. W. Beard and T. W. McLain, *Small Unmanned Aircraft - Theory and Practice*. Princeton University Press, 2012.